The main objective of this thesis has been the development of the required tools so as to design, simulate, fabricate and characterize any integrated optical device. From all the previous points, a special emphasis has been put on the simulation and the technological steps. For this reason, in chapter 5 the devices have not been exhaustively characterized, since the idea was to validate the simulation programs and the technological steps used.

It has been confirmed that the antiresonant pair underneath the core behaves as a Fabry-Perot, with periodical attenuation minimums as a function of the first cladding layer, which matches with the antiresonant conditions for the Fabry-Perot structure. Numerical methods for the optimization of ARROW structures have been developed. For analyzing the electromagnetic field in the cross-section, the NU-FDM algorithms have been implemented. Once the field profile was obtained, 3D analysis was firstly done by ways of the 2D-BPM. However, it was observed that required computational time was excessively large. This point, together with the fact that ARROW modes were strongly confined on the waveguides, i.e. they were far from cutoff conditions, suggested that the EIM could be used for reduce one dimension during the simulation of the structure, allowing using the much faster and simpler 1D-BPM .

Optimization of the ARROW structure was based on the defined external and internal asymmetry parameters, defined as $\Delta n_{ce}=n_c-n_{ext}$ and $\Delta n_{c2}=n_c-n_2$. Simulations confirmed that the minimum attenuation was obtained when both cladding satisfy the antiresonant conditions. They also showed that TM modes have much higher attenuation in ARROW-A structures, while it was not so in ARROW-B. This fact was associated to the different type of reflection done at the core-1st cladding boundary. For both polarizations, however, the light confinement inside the waveguide decreased as the core thickness diminishes. This fact provides with a minimum core size limit (4μm). It was confirmed that in ARROW-A structures, a competence between antiresonant and TIR confinement was produced. When $\Delta n_{ce}<0.6$ and $\Delta n_{c2}=0$, antiresonance prevails over TIR due to the fact that the refractive indexes between the core and the outer media (air) was relatively low. On the complementary region, that is, when $\Delta n_{ce}>0.6$ and $\Delta n_{c2}=0$, TIR prevailed over antiresonance, causing an increase of the losses since the evanescent tail reached the silicon substrate. ARROW-B structures did not present this

competence: As Δn_{ce} increased, the confinement increased in the same way as it did when the 1st cladding layer thickness was increased, changing its modal properties from antiresonance to TIR. Finally, simulations showed that small variation of the internal asymmetry parameter (Δn_{c2}) caused a dramatic decrease of the attenuation of all modes, causing a multimode behavior.

For the fabrication of silicon-based integrated optics components several technological processes for obtaining layers have been studied. Among them, the growth silicon oxide and the LPCVD deposited silicon nitride have been chosen as optimum for the 2nd and 1st cladding layer, respectively, due to the homogeneity, both in refractive index and thickness and the repeatability obtained. The high flexibility on tailoring the refractive index as a function of the deposition conditions has caused PECVD to be selected for depositing the waveguide core. It was found that sometimes the structure cracked due to excessive mechanical stresses, then, a mechanical study of the PECVD silicon oxide layers was engaged.

Research on mechanical properties headed towards decreasing as much as possible the mechanical stresses on the PECVD layers. For that reason, as-deposited and RTA annealed samples were studied. Mechanical stress, refractive index, thickness, FTIR spectra and ellipsometric spectrometry results were done. N_2O and SiH_4 were used as precursors. Ratio ($R=[N_2O]/SiH_4$) between both gases was varied between 2.2 and 55. Results show that it was possible to obtain refractive indexes between 1.46 and 1.95 and that layer thicknesses did not significantly affect on the refractive index, which confirms that refractive index is homogeneous in all the core layer. After RTA processes, a sharp increase of the refractive index for low R samples was obtained, that suggested the formation of Si nanoclusters.

It was observed that mechanical stresses linearly increased in absolute value as R increased. However, when an RTA process was done, a broken line was obtained. Using FTIR spectra, it was possible to determine that low R variations were due to Si-H bond breaking, which caused layer densification and shrinkage. For high R samples, Si-OH bonds were also broken, causing layer shrinkage. However, due to the fact that these samples were nearly stoichiometric, layer tend to internal reordering, trying to reach the basic tetrahedral structure of the silicon oxide. This fact caused the layer

expansion. Then, complementary effects happened for high R that prevented a large variation of mechanical stress after RTA. Finally, it was observed that a large variation of the stress, from convex to concave, was obtained during the first thermal cycle for high R samples. After successive cycles, stress tended to a straight line but remained positive. Only after RTA, the reordering was produced and stress changed its sign. It was also observed that samples with thermal cycles but without RTA were still able to react with the atmosphere, partially recovering the initial mechanical stress. Low R samples, on the contrary, show low stress variation during thermal cycles since Si-H bonds band need a higher energy to be dissociated. Actually, dissociation only was observable at temperatures of 600ºC, and it was required an RTA process to cause hydrogen effusion.

The characterization of the waveguides showed that total losses were independent of the waveguide width for values higher than 6μm for the ARROW-A and 10μm for the ARROW-B, with total losses values of 3.12dB and 5.23, respectively. It has to be noted, however, that these values not only include intrinsic losses, but also insertion losses, which were measure to be about 2.7dB. Thus, intrinsic losses were 0.45dB/cm and 1.62dB/cm for ARROW-A and ARROW-B, respectively. Near-field profiles showed that for wider waveguides, although it still was single mode in the y direction (the direction of the antiresonant pair), there were several lateral modes in the waveguides. Only waveguides with width below 8μm showed single mode behavior in the cross-section. Finally, losses as a function of the wavelength were studied, showing that the minimum losses were obtained at the working wavelength. This fact confirms that all layer thickness and all refractive indexes matched with the requested specifications.

It has been seen that by adding Lateral Antiresonant Structures (LAS) over the slab ARROW structure, an antiresonant configuration with effective refractive indexes could be defined. Its major advantage of the ARROW-2D structures is the single mode behavior for large core widths. Moreover, since the confining in these structures is much lower as these of the rib structure, several LAS can be added, increasing its lateral confinement. Experimental results with these waveguides have shown that total losses were 7.53dB and 6.14dB for ARROW-2D structures with single and double LAS on

each side of the core. Near field profiles obtained have confirmed that waveguides up to 20μm wide present single mode behavior in the cross section.

The simulation of rib directional couplers using ARROW structures show that the coupling length exponentially increases as the distance between waveguides increased. Coupling length behavior as a function of the waveguide width showed two different regions: for narrow waveguides, non-linear behavior of the directional coupler was obtained. For relatively width waveguides, however, the expected linear increase as a function of the waveguide width was observed. Experimental results with an ARROW-B based directional coupler showed the expected periodical exchange of power between the waveguides as a function of the propagating distance. However, its period was significantly different as compared to the simulations. Scanning electron microscopy pictures done at the waveguides shown that the rib was not completely vertical, but has a tilt of 80º. If this geometrical parameter was added to the simulations, they match much better with experimental results. Actually, it was observed that coupling length could vary a 100% if identical waveguides but one with 45º and the other with 90º wall tilt, were compared. Finally, power obtained at the device output as a function of the wavelength for a fixed directional coupler length was studied. The periodical behavior obtained confirmed that the device was working correctly.

On the basis of ARROW-2D structures, directional couplers were also studied. It has been observed that the coupling length as a function of the distance between waveguides does not increase exponentially, but has a periodical response. This behavior can be associated to the fact that coupling is done by ways of radiate waves. Which is poorly dependent of. the separation between them. The optimal configuration for the directional coupler using ARROW-2D structures would consist on a double LAS in the outer part of the waveguide, which would assure the optical confinement in the waveguide, and single LAS at the inner regions, in order to enhance coupling. Simulations have provided information either of the coupling and the power exchange between remote waveguides. Experimental results have confirmed the power exchange between remote waveguides. However, the absence of a reference waveguide has prevented to determine the ARROW-2D directional coupler losses. Near field images, however, have confirmed the coupling between the waveguides.

It has been observed that straight Y-junctions present higher losses due to poor modal matching. By replacing straight by bent structures, losses can be significantly reduced. However, the sharp edge where both output waveguides are connected cannot be obtained by single mask lithographic definition, and the uncontrolled blunted vertex causes unbalanced power transfer at the waveguides. Several proposals have been made in order to overcome this problem, either using 1x2 rib or 1x2 ARROW-2D directional couplers and 1x2 multimode interference couplers. It has to be noted that these latter structures, although need technological accuracy, are selective to the wavelength. The absence of vertex and small parts in its geometries grants that technology would provide with optimum results. However, its major drawback is that they require precise alignment. A complementary structure, based on parabolic horns, provides with a structure having low loss, no blunted vertex and does not require accurate alignment. When comparing experimental results of straight and bend Y-junctions, 1x2 directional couplers and U-junctions, it has been observed that the latter have much lower unbalance (0.83%) and a much larger tolerance to misalignment as compared to the others.

On the basis of the previous 3dB splitters, Mach Zehnder structures based on combinations of bend Y-junctions, rib directional couplers and U-junctions were proposed. So far, only standard Y-Y junctions have been fabricated and tested. It was observed that the mode in the waveguide could be pushed towards the upper part of the waveguide without loosing its confining properties if a thin layer was placed over the waveguide. After reducing the core dimension to 3μm and depositing 35nm of silicon nitride on the sensing region, the system was able to detect variations of the refractive index of 4.10^{-7}, which allows detecting bio-molecular reactions.

The second generation of the optochemical sensor was also developed, with both input and output waveguides on the same side. This has been achieved by making a 180º bend on one waveguide. It was observed that in pure bend waveguides, losses decreased as the width increased. However, it was also observed that in the bend region, mode was displaced towards the exterior of the waveguide and thus, in the bend-straight region, transition losses were much higher in the wider waveguides since the modal profiles did not match. Thus, an agreement must be reached between losses at the bend

region and losses due to bend-straight modal mismatch. 20μm input waveguides with 3 different bend radius: 2, 4 and 6mm were defined on the masks. The output waveguide has a width of 60μm, this waveguide assures maximum light collecting. The second requirement was the avoiding of alignment. This was achieved by a three-pieced system: the sensor, in which deep channels on silicon were done, the V-grooves, where input and output fiber optics were located, and the aligner chip, that was glued to the V-grooves and assured appropriate aligning between the fiber optics and the waveguides. It was observed that the system was able to measure potassium-ion concentrations up to 10^{-4}M, with an extremely large range of absorbance (3 units). Moreover, the optochemical sensor was completely reversible.

It was observed that in order to have the same dynamical range when measuring positive and negative acceleration values, beam divergence should be taken into account in diaphragm accelerometers. When the diaphragm is half covering the output waveguide, simulated power losses were not the expected 3dB, but 5.22dB. Thus, waveguides were put as close as possible (50μm), which provided a linear range of 1.6μm. However, for security purposes, it was reduced to 1μm. Optical considerations were used as the starting point for the mechanical considerations. The quad-beam structure was chosen as optimum since it allowed flat mass displacement. Beam lengths and mass size were designed appropriately so as to detect up to 50g with a opto-mechanical sensitivity of 9dB/μm. It was observed that due to its configuration, the device was not sensitive to crossed accelerations in x axis. However, this magnitude was the 20% of the value obtained in the active axis (z). This factor should be taken into account in the measurements. Finally, resonant frequencies for the several vibration modes were also calculated, being 4.945Khz for the first mode.

During the last steps in the fabrication process, waveguides should be protected when etching the buried silicon oxide layer of the BESOI wafer. Photoresist, silicon nitride and polysilicon were used as masks. However, due to the high steps of the structure, step coverage was not good enough an HF also etched the waveguide. This problem, still unsolved, has prevented from obtaining the diaphragm uniaxial optical accelerometer.

Misalignment accelerometer is simpler as compared to the diaphragm accelerometer. Its configuration, although prevented from differentiates between positive and negative accelerations, had a larger span (μm) as compared to the previous accelerometer. Beam divergence was corrected in the waveguide cross section, either by progressively increasing the waveguide width or by placing the frame and the seismic mass as close as possible. It was also observed that the structure was self-aligned and had an auto-test system, since were the mass to be broken, losses as high as 45 dB would be obtained. Identically to the diaphragm accelerometer, optical considerations were applied to the mechanical design of the beams and the seismic mass. In this case, however, beams were done larger and mass wider since the it was designed to measure up to 1g, with a sensitivity of 4.5dB/μm. Again, due to geometrical considerations, crossed accelerations in the y axis did not affect the measurement. However, similarly to what happened with the diaphragm accelerometer, the crossed acceleration in the x axis was significantly high (20%). Resonant frequencies for the different vibrational modes are much lower (0.489Khz for the first mode) since the working regime requires a much flexible structure.

During the assembly of the components (waveguides and V-grooves), it was observed that high insertion losses were obtained, which have been associated to an inappropriate alignment or to defects during polishing. Nevertheless, although sensitivity was ½ of the theoretical, it was still possible to characterize the devices, showing the expected periodical variation of power when their relative angle with the gravitational field changed. From the data obtained, it was observed that waveguides were only 0.18μm misaligned. Linear range was obtained in according to the simulations. However, an asymmetrical behavior, depending on the sign of the gravity, was obtained due to the passivation effects. This fact has been confirmed with the dynamical measurements. When applied a periodical excitation, a power output with half period was obtained. This point agrees with the fact that, in a period, waveguide on the seismic mass crosses twice the region where is maximum power. Again, it can be observed that beats have slight different amplitude. This matches with the previous measurements, showing that the accelerometer has an asymmetrical response for large positive and negative g.

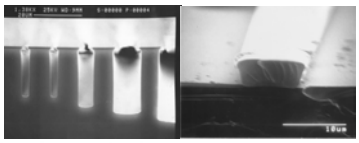

Stabilization of a technology for obtaining silicon-based ARROW structures in the visible range has been developed and confirmed by several devices. However, near and mid-IR range, core thickness in an equivalent ARROW configuration requires a core of at least 7μm thick, with a 2nd cladding layer of 3.5μm. A PECVD deposited layer of this thickness would have large desuniformity and probably crack due to excessive mechanical stresses. Two different research lines have been recently engaged for obtaining integrated optical devices for telecommunication wavelengths.

Polymer waveguides

Organic polymers are becoming an attractive choice for integrated optical waveguides on semiconductor substrates, in particular, on silicon. It has proven to be appropriate for many integrated optical devices, as couplers, modulators and sensors. Polymers have the advantages over inorganic materials in terms of process and cost. In fact, polymer-based waveguide devices are expected to be one of the key points in the next generation of optical fiber telecommunications.

Recently, in collaboration with Microchem®, it has been engaged a set of experiments with SU-8 2000 negative-tone photoresist in order to obtain polymer-based waveguides. Three different configurations are under test. All of them are hybrid structures, since they require both the polymer and the silicon oxide layers.

	Core (d_c)	1st Cladding (d_1)	2nd Cladding (d_2)
ARROW-1	Polymer	Silicon oxide	Polymer
ARROW-2	Polymer	Silicon oxide	Silicon oxide
TIR-1	Polymer	Silicon oxide	

With the first set of SU-8 2005 samples, it was possible to determine its refractive index at 633nm. Layers with a hard bake of 200ºC and 300ºC were measured, having refractive index values of 1.57±0.02 and 1.71±0.04, respectively and negligible absorption. This was a very promising result since it would mean that losses were significantly reduced as compared to the first process, at least in the 633nm region. Then, TIR polymer-based waveguides were fabricated, as shown in fig. 1. They presented a slight negative wall and high roughness at the facets. In order to diminish

the roughness, it was tried to polish the waveguides. Unfortunately, they did not stand the process and were severely damaged. This fact confirms that the technological process was not optimized and that a further research is required.

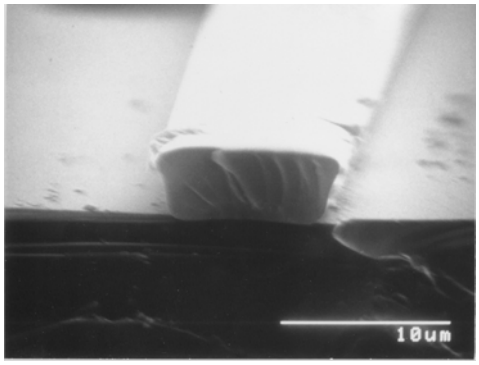

Fig. 1: SEM microphotographs of a SU-8 2005 waveguide

Losses as a function of the wavelength were measured for 60µm width waveguides with their facets not polished. As can be seen in fig. 2, minimum losses of 5.23dB were observed at 1300nm. There also exist two sharp peaks, located at 650 and 1550nm. Being the second is probably due to incomplete solvent effusion, causing a high content of –OH bonds in the waveguide, again confirming that the technological process, probably the hard bake, is not optimized yet.

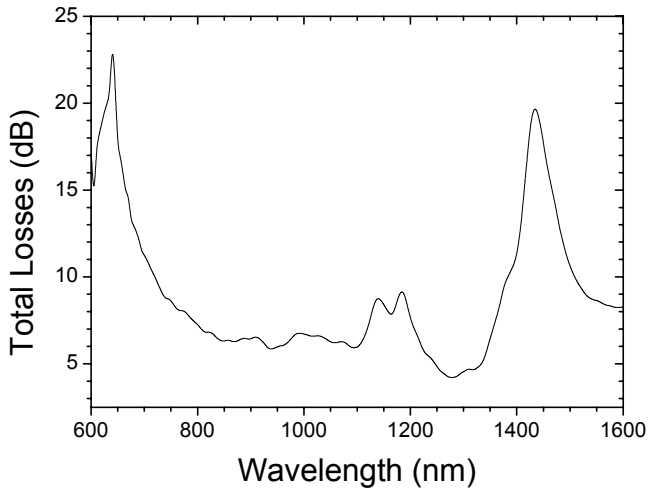

Fig. 2: Losses as a function of the wavelength for 60µm-width polymer waveguides.

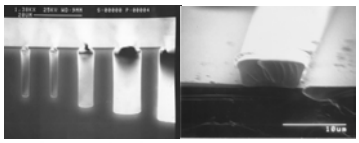

Despite losses were excessively large value, it has to be taken into account that these waveguides were unable to be polished. Then, insertion losses should be quite high. Nevertheless, as far as waveguides was concerned, it was an excellent beginning.

Hollow waveguides

The second research line that has recently started is based on hollow silicon waveguides, as compared to solid ones, two significant differences can be observed. The first and the most obvious, that the core material is replaced by a gas or vacuum. The second, is that the cladding of a hollow waveguide commonly is absorbent at the working wavelength. Highly opaque materials could then be used as long as the gas within the core is transparent. As far as walls are concerned, its roughness has to be as small as possible in order to have specular behavior. In order to assure this last behavior, reflecting surfaces can cover them. Generally, these types of structures are used for high power laser delivery, working at mid-IR wavelengths (10.6μm). This is a major drawback for using low melting point glasses, since laser heating and damage could be very high.

With the well-known silicon micromechanization technology, it has been possible to obtain the first si-based hollow waveguides, shown in fig. 3. The cover wall could be an anodically bonded Si wafer. Moreover, it would also be possible to define several other devices on the same chips, as could be cooling systems along the waveguide, if necessary, in order to avoid overheating.

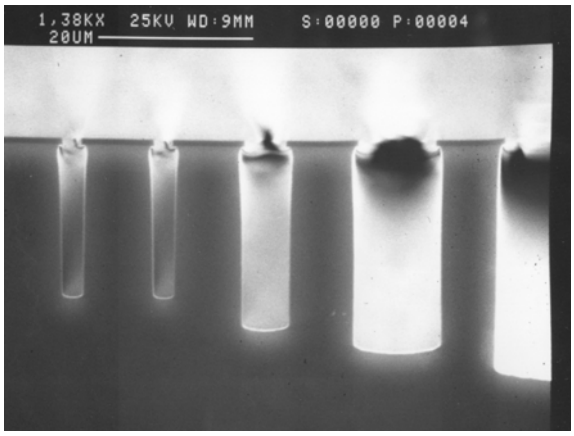

Fig. 3: SEM microphotographs of the first Si-based hollow waveguides

It has to be noted that this type of waveguides has many interesting applications, as could be: Surgical CO_2 or Er:YaG Laser power delivery, Industrial metal processing, military counter measures, signal delivery, thermometry, imaging and spectrometry.